A simple optical coherence tomography quantification method for choroidal neovascularization

Rania S. Sulaiman[1,2,3,6], Judith Quigley[1,2], Xiaoping Qi[1,2], Michael N. O'Hare[1,2,7] Maria B. Grant[1,2], Michael E. Boulton[1,2,], Timothy W. Corson[1,2,3,4,5 *]

[1]Eugene and Marilyn Glick Eye Institute, [2]Department of Ophthalmology, [3]Department of Pharmacology and Toxicology, [4]Department of Biochemistry and Molecular Biology, Indiana University School of Medicine, Indianapolis, Indiana, [5]Indiana University Melvin and Bren Simon Cancer Center, Indianapolis, Indiana, [6]Department of Biochemistry, Faculty of Pharmacy, Cairo University, Cairo, Egypt, [7]School of Biomedical Science, University of Ulster, Coleraine, Northern Ireland, United Kingdom

*Corresponding author, e-mail; tcorson@iupui.edu, Phone: +1–317–274–3305, Fax: +1–317–274–2277, Address: 1160 West Michigan Street, Indianapolis, IN 46202

Running title: OCT quantification of CNV volume

Word count: 2705

Keywords: Optical coherence tomography, choroidal neovascularization, ophthalmic imaging, laser-induced CNV, animal models, quantitative analysis

This is the author's manuscript of the article published in final edited form as:
Sulaiman, R. S., Quigley, J., Qi, X., O'Hare, M. N., Grant, M. B., Boulton, M. E., & Corson, T. W. (2015). A Simple Optical Coherence Tomography Quantification Method for Choroidal Neovascularization. Journal of Ocular Pharmacology and Therapeutics. http://dx.doi.org/10.1089/jop.2015.0049

Sulaiman, R.S.

Abstract

Purpose: Therapeutic efficacy is routinely assessed by measurement of lesion size using flatmount retinas and confocal microscopy in the laser-induced choroidal neovascularization (L-CNV) rodent model. We investigated whether optical coherence tomography (OCT) quantification, using an ellipsoid volume measurement, was comparable to standard ex vivo evaluation methods for this model and whether this approach could be used to monitor treatment-related lesion changes.

Methods: Bruch's membrane was ruptured by argon laser in the dilated eyes of C57BL/6J mice, followed by intravitreal injections of anti-$VEGF_{164}$ or vehicle, or no injection. In vivo OCT images were acquired using Micron III or InVivoVue systems at 7, 10, and/or 14 days post-laser and neovascular lesion volume was calculated as an ellipsoid. Subsequently, lesion volume was compared to that calculated from confocal Z-stack images of agglutinin stained choroidal flatmounts.

Results: Ellipsoid volume measurement of orthogonal 2D OCT images obtained from different imaging systems correlated with ex vivo lesion volumes for L-CNV (Spearman's ρ = 0.82, 0.75, and 0.82 at days 7, 10, and 14, respectively). Ellipsoid volume calculation allowed temporal monitoring and evaluation of CNV lesions in response to anti-VEGF treatment.

Conclusions: Ellipsoid volume measurements allow rapid, quantitative use of OCT for assessment of CNV lesions in vivo. This novel method can be used with different OCT

imaging systems with sensitivity to distinguish between treatment conditions. It may serve as a useful adjunct to the standard ex vivo confocal quantification, to assess therapeutic efficacy in preclinical models of CNV, and in models of other ocular diseases.

Introduction

Choroidal neovascularization (CNV) is the aberrant growth of new blood vessels originating from the choroid into the subretinal space through a break in Bruch's membrane.[1] These new vessels can lead to vascular leakage, hemorrhage, formation of fibrovascular membranes, retinal detachment and eventually, if not treated, to a fibrous scar.

CNV is a major cause of visual loss and is implicated in several neovascular eye diseases such as the wet (or exudative) form of age-related macular degeneration (AMD).[2] Wet AMD is responsible for about 90% of AMD-related blindness in individuals over the age of 55, with about 200,000 new cases diagnosed every year in the United States alone.[3, 4] Laser-induced CNV (L-CNV) is a frequently used experimental technique in mice and rats that induces breaks in Bruch's membrane and stimulates blood vessel growth from the choriocapillaris.[5] The resultant CNV resembles aspects of exudative AMD and can easily be performed in rodents, producing robust subretinal vascular lesions within 14 days. L-CNV has become the "gold standard" in preclinical studies,[6] despite limitations of using rodents.[5] This model has been invaluable for the evaluation of the effects of drug therapies on CNV lesion progression[7, 8]

Vascular endothelial growth factor (VEGF) has been recognized as a key proangiogenic factor in CNV. Targeting the VEGF pathway, using specific antibodies, antibody fragments, or aptamers, is a standard pharmacotherapeutic approach for wet AMD[9] and has been previously tested in L-CNV experimental models.[10, 11] Several methods for 2-

dimensional (2D) evaluation of L-CNV lesions have been used including histological analysis and fluorescein angiography.[12] Measuring L-CNV lesion volume using stained choroidal flatmounts ex vivo allows 3-dimensional (3D) measurement of lesion size, which is more informative than measuring lesion area alone and has become widely accepted as a quantitative method to indicate drug efficacy in ameliorating CNV lesions.[5, 13, 14]

Although ex vivo lesion measurements of L-CNV are robust and powerful, in vivo imaging analysis of lesions would allow longitudinal studies. Optical coherence tomography (OCT) is a non-invasive, in vivo imaging technique that generates high resolution, cross sectional images of biological systems.[15] The technique has found extensive use in ophthalmology[15, 16] providing detailed images for both the anterior and posterior segments of the eye[17] and has become an essential tool for the clinical evaluation of ocular pathologies such as wet AMD,[18] retinal tumors,[19-21] and retinal detachment.[22]

Paralleling its rise to clinical prominence, OCT has been used preclinically to monitor disease progression, and OCT images have been shown to be comparable to histological characteristics in disease models,[23-26] including L-CNV.[12, 27] However, to our knowledge, 3D quantification of lesions in OCT images has previously used specialized software that is not readily available or compatible with different systems. Moreover, the correlation between calculated lesion volume from OCT images and ex vivo choroidal flatmount 3D quantification has not been shown previously. In this study, we show that

simple quantification of lesion volumes from OCT images provides reproducible and comparable evaluation to the ex vivo analytical methods used in the L-CNV mouse model.

Methods

Animals

All animal experiments followed the guidelines of the Association for Research in Vision and Ophthalmology Statement for the Use of Animals in Ophthalmic and Vision Research and were approved by the Indiana University School of Medicine Institutional Animal Care and Use Committee. Wild-type female C57BL/6J mice, 6–8 weeks of age, were purchased from Jackson Laboratory (Bar Harbor, ME). These mice were anesthetized by intraperitoneal injections of 17.5 mg/kg ketamine hydrochloride and 2.5 mg/kg xylazine.

Laser-Induced model of Choroidal Neovascularization

Laser photocoagulation was performed as previously described.[28, 29] Briefly, eyes were dilated using 1% tropicamide, then underwent laser treatment using 50 μm spot size, 50 ms duration, and 250 mV pulses of an ophthalmic argon green laser, wavelength 532 nm, coupled to a slit lamp. A coverslip was used to allow viewing of the posterior pole of the eye. Each eye received 3 laser burns centered around the optic nerve at 12, 3, and 9 o'clock positions. The laser-induced damage to Bruch's membrane was identified by the appearance of a bubble at the site of laser application. Lesions in which bubbles

were not observed were excluded from the study. Where indicated, intravitreal injections of anti-mouse $VEGF_{164}$ neutralizing antibody (R&D Systems, Minneapolis, MN) (5 ng/eye) or vehicle (phosphate buffered saline) were given immediately after laser in a 0.5 μL volume using a 33-gauge needle. The needle was kept in place for 1 minute to prevent the reflux of solution when the needle was removed. Eyes were numbed with tetracaine solution before the injection, and triple antibiotic ointment was used immediately after the injection to prevent infection. A masked researcher undertook imaging and analysis to avoid bias.

Optical Coherence Tomography

OCT was performed at the indicated times using the Micron III intraocular imaging system (Phoenix Research Labs, Pleasanton, CA) or the InVivoVue OCT system (Bioptigen Inc., Research Triangle Park, Durham, NC). These are the two most commonly used rodent OCT systems. For the Micron system, imaging was done by a single experimenter (RSS). Before the procedure, eyes were dilated with 1% tropicamide solution and lubricated with hypromellose ophthalmic demulcent solution (Gonak) (Akorn, Lake Forest, IL). Mice were then placed on a custom heated stage that moves freely to position the mouse eye for imaging. Several horizontal and vertical images were taken per lesion to allow calculation of CNV lesion volume.

For the InVivoVue system, experiments were done separately by a second laboratory, with imaging conducted by JQ. Pupils of mouse eyes were dilated with 1% atropine and 2.5% phenylephrine hydrochloride. Mice were then anesthetized. One drop of 2.5% hydroxypropyl methylcellulose was administrated to eyes before examination. Three

lateral images (nasal to temporal) were collected, starting at the meridian crossing through the center of the optic nerve head (ONH), and the corresponding L-CNV injury spots were identified by contrasts. Composite fundus images (1.4x1.4 mm, 400x100x1x1) were taken centered on the ONH. Corresponding high resolution B-scan (1.4x1.4 mm, 400x400x1x1) images were then obtained from swept L-CNV spots.

Quantification of Lesions as Ellipsoids

Quantification was performed as in Fig. 1, for images obtained from the Micron system. The widest section of the lesions from perpendicular planes were used to calculate ellipsoid volume using the formula $V = \frac{4}{3}\pi abc$ where a, b, and c are the radii of the three axes of the ellipsoid. The radii were manually drawn and measured using ImageJ software. The CNV lesion borders were defined from the onset of thickening of the choroidal layer horizontally to the borders of the hyperreflective lesion vertically. The lesion borders were defined similarly for images obtained using the InVivoVue system. In this case, quantitative measures, width (a) and depth (b) of the lesion were measured from the exported central image in B-scanned compositions. The length (c) of the lesions was calculated from en face images as the difference in distance between the beginning and the end of the lesion. Images from both the Micron III and InVivoVue systems were analyzed by two independent graders (RSS and MNO) for interobserver comparison. The volumes of the three lesions in each eye were averaged and considered as an n=1 for statistical analysis.

Choroidal flatmount preparation and ex vivo CNV lesion volume quantification

Fourteen days post-laser, L-CNV mice were euthanized by carbon dioxide asphyxiation followed by cervical dislocation. Eyes were enucleated and fixed in 4% paraformaldehyde (PFA) overnight. The anterior segment and the retina were removed, and the remaining RPE/choroid/sclera was permeabilized by incubation with 0.3% Triton X-100 followed by incubation with rhodamine labeled *Ricinus communis* agglutinin I (Vector Labs, Burlingame, CA), in the dark for 45 minutes, to stain blood vessels. The staining step was followed by two washes with Tris buffered saline with 0.1% Tween-20 (TBST). Flatmounts of the choroid were prepared and mounted with Vectashield mounting medium (Vector Labs, Burlingame, CA) and Z-stack images were taken on an LSM700 confocal microscope (Zeiss, Thornwood, NY, USA). ImageJ software was used to analyze Z-stack images; the summation of the whole stained area in each section, multiplied by the distance between sections (3 μm) was used as an index for the CNV lesion volume.[28] The volumes of the three lesions in each eye were averaged and considered as an n=1 for statistical analysis.

Statistical analysis

Statistical analysis was performed with GraphPad Prism 6 software. CNV volume was compared between treatments using the Mann-Whitney test. The Spearman correlation coefficient was used to assess the correlation between lesion volumes measured by

OCT and choroidal flatmounts. P-values ≤ 0.05 were considered statistically significant.

Results

Ellipsoid quantification in vivo is comparable to ex vivo analysis in L-CNV

Although Z-stack analysis of wholemounts gives robust and reproducible data, we sought a simple means of evaluating L-CNV lesion volume in vivo. Mice underwent OCT 14 days post-laser. Comparing volumetric measurements of OCT and agglutinin-stained wholemount Z-stacks, significant correlation was observed by two independent graders; grader 1 with $\rho = 0.79$, $P<0.01$ and grader 2 $\rho = 0.78$, $P<0.05$ (Fig. 2). The intraobserver correlation (based on repeated analysis of the same dataset) was $\rho = 0.9$, $P<0.001$, while the interobserver correlation was $\rho = 0.73$, $P<0.05$.

Ellipsoid quantification is sensitive to different treatment conditions

In the L-CNV model, anti-VEGF antibodies have previously been shown to reduce CNV lesion volume, based on Z-stack image quantification, compared to vehicle treated controls.[30] We first sought to reproduce this amelioration in the CNV lesion size using the L-CNV mouse model and to compare the difference between treatment groups using both confocal microscopy and OCT. Quantification of CNV lesion volume using the standard Z-stack image method showed the expected significant reduction, about 35%,[31] in lesion volume after anti-VEGF treatment compared to vehicle controls (Fig. 3).

Interestingly, CNV lesion volume calculated using this method from OCT images obtained 7 days after laser and injection also demonstrated a significant reduction, likewise about 35%, after anti-VEGF treatment (Fig. 4). Similar results were obtained from images after 14 days (Fig. 4). Importantly, OCT volume measurements significantly correlated with those measured by Z-stack quantification, after 7 days ($\rho = 0.82$, $P<0.01$) (Fig. 5A), and after 14 days ($\rho = 0.82$, $P<0.01$) (Fig. 5B).

Ellipsoid quantification is OCT platform-independent

To validate that our ellipsoidal volume measurement technique could be applied to images from another automated OCT system, we evaluated L-CNV lesions using OCT images obtained with the InVivoVue system. Laser burns were applied to mouse eyes and after 10 days, lesions were evaluated by OCT in vivo. Lesion volumes were calculated by ellipsoid volume equation, and again compared to volumetric measurements of CNV lesion volumes from agglutinin stained choroidal flatmounts ex vivo after 14 days. Interestingly, a significant correlation was again observed between ellipsoid volume calculation and confocal Z-stack images (Fig. 6) ($\rho = 0.75$, $P<0.05$). Similar correlation values were obtained by a second grader to account for interobserver variability (data not shown). Moreover, removing the peak point, which might be an outlier, did not change the correlation ($\rho = 0.75$, $P<0.05$).

Discussion

OCT imaging represents an essential adjunct in clinical diagnosis and monitoring of numerous ocular diseases, such as AMD.[20, 32] Evaluation of L-CNV in vivo using OCT

imaging has been previously studied in different species such as monkeys,[33, 34] rabbits,[35] and rats.[27, 36, 37] Others have evaluated OCT in the mouse model of L-CNV used here by comparing OCT imaging to immunostaining and histological analyses.[12, 38, 39] However, in this study, we compared for the first time OCT quantification of L-CNV lesions to the robust and commonly used ex vivo agglutinin stained choroidal wholemount quantification method, which allows volumetric measurements of L-CNV lesions through Z-stack sections.[5, 13] We saw excellent correlation between the two methods using different OCT imaging systems.

Quantification of OCT images usually requires specialized, proprietary software that is not necessarily compatible with multiple imaging systems. In this study, we showed that quantitative OCT analysis by a simple method allowed in vivo evaluation and monitoring of choroidal lesions in the L-CNV model using two of the most commonly used OCT imaging systems. Although we used ImageJ for analysis, the radii measurements needed for ellipsoid volume could be done using any image-editing program. Quantification of L-CNV lesions, obtained from either Micron or InVivoVue OCT images, using an ellipsoid volume calculation, provides reproducible and comparable results to the standard ex vivo quantification method. Consistently, we observed a significant correlation, by two independent graders, between OCT images obtained at day 7, 10, or 14 post-laser, and Z-stack confocal measurements at day 14. However, due to the difference in scaling of the Micron III and InVivoVue imaging systems; calculated lesion volumes by Micron OCT were uniformly larger than those calculated by confocal microscopy. Tissue shrinkage during fixation may also contribute to this finding.

Alternatively, since the length of the lesion (dimension *c*) on the InVivoVue was obtained from en face images directly, not from vertical scans as was done with the Micron III system, this might induce some differences in the final calculation. Thus, using the same volumetric measurement system throughout the analysis of an experiment is important.

Our method also applies to OCT imaging to assess pharmacotherapeutic efficacy. Here, as proof of concept, we used the standard anti-VEGF antibody treatment, versus vehicle treatment, to ameliorate CNV lesion volume. To our knowledge, this is the first use of OCT to show therapeutic effect in the murine L-CNV model, although OCT has been used similarly in macaques.[34] As we show, OCT can be used to monitor drug response longitudinally in the same animal, reducing animal usage and enabling time-course comparisons. For instance, we noted that mean L-CNV lesion volumes decreased from Day 7 to Day 14 (Fig. 4, 5), but the distinction between anti-VEGF and vehicle treatments remained about 35% as previously shown.[31]

OCT analysis is also rapid. Preparation of choroidal flatmounts for the quantification of L-CNV lesion volume is a technically involved and time-consuming technique, requiring at least one overnight step and considerable confocal imaging time, as well as expensive reagents (fluorescent agglutinin in particular).[5] Conversely, acquiring multiple images on an OCT system takes about 5 –10 minutes per eye followed by 5 minutes for calculation of the lesion volume. Therefore, our ellipsoid volume quantification method represents an inexpensive, rapid, yet reliable quantification method for lesions from

OCT images. Despite that, it is important to mention that OCT quantification is not a replacement for the Z-stack confocal measurement. However, it might provide an early prediction of therapeutic effects as well as a second evaluation method for CNV lesion volume.

One limitation of this method is the manual detection of CNV lesion dimensions, which might introduce bias to treatment conditions. However, this can be avoided when the experimenter is masked to treatments throughout imaging and analysis, as well as using at least two independent graders for volumetric analysis. True CNV lesion shape is likely not a simple ellipsoid; therefore, using a simple ellipsoid volume measurement may overestimate irregularly shaped lesions.[39] However, following from this, in experiments comparing CNV-lesion reducing therapies to control conditions it is likely that our method would be quite conservative (by potentially *overestimating* lesion volume and thus *underestimating* treatment effects), which might be considered as a strength. Like any OCT analysis, our method also requires a clear cornea and lens, and lesions in or near the central retina. This method is also limited to disease models that involve localized lesions that can be demarcated by OCT, such as L-CNV. However, a strength of our method is that it can be used to calculate volumes from the L-CNV murine model using different automated imaging systems, specifically the Micron and InVivoVue products.

This study provides evidence that OCT is a valuable tool to rapidly and quantitatively evaluate response to drug therapies for choroidal neovascularization using the L-CNV

mouse model. Our simple ellipsoidal quantification method may also be applied to the analysis of other focal intraocular lesions and provides rapid analysis for preclinical testing of possible therapeutic agents.

Acknowledgements

This work was supported by the International Retinal Research Foundation, the Retina Research Foundation, and an unrestricted grant from Research to Prevent Blindness, Inc. TWC is supported by NIH KL2TR001106. MEB is supported by R01EY018358. MBG is supported by R01HL110170-03, R01EY007739-23, R01EY012601-15, and R01DK090730-04.

Author disclosure statement

TWC has received research and travel support from Phoenix Research Labs. No competing financial interests exist for the other authors.

References

1. de Jong PT. Age-related macular degeneration. *N Engl J Med*. 2006; 355:1474-1485.
2. Jager RD, Mieler WF, Miller JW. Age-related macular degeneration. *N Engl J Med*. 2008; 358:2606-2617.
3. Congdon N, O'Colmain B, Klaver CC, et al. Causes and prevalence of visual impairment among adults in the United States. *Arch Ophthalmol*. 2004; 122:477-485.
4. Grossniklaus HE, Green WR. Choroidal neovascularization. *Am J Ophthalmol*. 2004; 137:496-503.

5. Lambert V, Lecomte J, Hansen S, et al. Laser-induced choroidal neovascularization model to study age-related macular degeneration in mice. *Nat Protoc*. 2013; 8:2197-2211.
6. Grossniklaus HE, Kang SJ, Berglin L. Animal models of choroidal and retinal neovascularization. *Prog Retin Eye Res*. 2010; 29:500-519.
7. Dobi ET, Puliafito CA, Destro M. A new model of experimental choroidal neovascularization in the rat. *Arch Ophthalmol*. 1989; 107:264-269.
8. Sulaiman RS, Basavarajappa HD, Corson TW. Natural product inhibitors of ocular angiogenesis. *Exp Eye Res*. 2014; 129:161-171.
9. Prasad PS, Schwartz SD, Hubschman JP. Age-related macular degeneration: current and novel therapies. *Maturitas*. 2010; 66:46-50.
10. Saishin Y, Saishin Y, Takahashi K, et al. VEGF-TRAP(R1R2) suppresses choroidal neovascularization and VEGF-induced breakdown of the blood-retinal barrier. *J Cell Physiol*. 2003; 195:241-248.
11. Krzystolik MG, Afshari MA, Adamis AP, et al. Prevention of experimental choroidal neovascularization with intravitreal anti-vascular endothelial growth factor antibody fragment. *Arch Ophthalmol*. 2002; 120:338-346.
12. Giani A, Thanos A, Roh MI, et al. In vivo evaluation of laser-induced choroidal neovascularization using spectral-domain optical coherence tomography. *Invest Ophthalmol Vis Sci*. 2011; 52:3880-3887.
13. Sengupta N, Caballero S, Mames RN, et al. The role of adult bone marrow-derived stem cells in choroidal neovascularization. *Invest Ophthalmol Vis Sci*. 2003; 44:4908-4913.
14. Sengupta N, Caballero S, Mames RN, et al. Preventing stem cell incorporation into choroidal neovascularization by targeting homing and attachment factors. *Invest Ophthalmol Vis Sci*. 2005; 46:343-348.
15. Huang D, Swanson EA, Lin CP, et al. Optical coherence tomography. *Science*. 1991; 254:1178-1181.
16. Chen TC, Cense B, Pierce MC, et al. Spectral domain optical coherence tomography: ultra-high speed, ultra-high resolution ophthalmic imaging. *Arch Ophthalmol*. 2005; 123:1715-1720.
17. Drexler W, Morgner U, Ghanta RK, et al. Ultrahigh-resolution ophthalmic optical coherence tomography. *Nat Med*. 2001; 7:502-507.
18. Jia Y, Bailey ST, Wilson DJ, et al. Quantitative optical coherence tomography angiography of choroidal neovascularization in age-related macular degeneration. *Ophthalmology*. 2014; 121:1435-1444.
19. Espinoza G, Rosenblatt B, Harbour JW. Optical coherence tomography in the evaluation of retinal changes associated with suspicious choroidal melanocytic tumors. *Am J Ophthalmol*. 2004; 137:90-95.
20. Rootman DB, Gonzalez E, Mallipatna A, et al. Hand-held high-resolution spectral domain optical coherence tomography in retinoblastoma: clinical and morphologic considerations. *Br J Ophthalmol*. 2013; 97:59-65.
21. Shields CL, Pellegrini M, Ferenczy SR, Shields JA. Enhanced depth imaging optical coherence tomography of intraocular tumors: from placid to seasick to rock and rolling topography--the 2013 Francesco Orzalesi Lecture. *Retina*. 2014; 34:1495-1512.

22. Wolfensberger TJ, Gonvers M. Optical coherence tomography in the evaluation of incomplete visual acuity recovery after macula-off retinal detachments. *Graefes Arch Clin Exp Ophthalmol*. 2002; 240:85-89.
23. Fischer MD, Huber G, Beck SC, et al. Noninvasive, in vivo assessment of mouse retinal structure using optical coherence tomography. *PLoS One*. 2009; 4:e7507.
24. Huber G, Beck SC, Grimm C, et al. Spectral domain optical coherence tomography in mouse models of retinal degeneration. *Invest Ophthalmol Vis Sci*. 2009; 50:5888-5895.
25. Corson TW, Samuels BC, Wenzel AA, et al. Multimodality imaging methods for assessing retinoblastoma orthotopic xenograft growth and development. *PLoS One*. 2014; 9:e99036.
26. Wenzel AA, O'Hare MN, Shadmand M, Corson TW. Optical coherence tomography enables imaging of tumor initiation in the TAg-RB mouse model of retinoblastoma. *Mol Vis*. 2015; In press.
27. Fukuchi T, Takahashi K, Shou K, Matsumura M. Optical coherence tomography (OCT) findings in normal retina and laser-induced choroidal neovascularization in rats. *Graefes Arch Clin Exp Ophthalmol*. 2001; 239:41-46.
28. Qi X, Cai J, Ruan Q, et al. γ-Secretase inhibition of murine choroidal neovascularization is associated with reduction of superoxide and proinflammatory cytokines. *Invest Ophthalmol Vis Sci*. 2012; 53:574-585.
29. Sengupta N, Afzal A, Caballero S, et al. Paracrine modulation of CXCR4 by IGF-1 and VEGF: implications for choroidal neovascularization. *Invest Ophthalmol Vis Sci*. 2010; 51:2697-2704.
30. Campa C, Kasman I, Ye W, et al. Effects of an anti-VEGF-A monoclonal antibody on laser-induced choroidal neovascularization in mice: optimizing methods to quantify vascular changes. *Invest Ophthalmol Vis Sci*. 2008; 49:1178-1183.
31. Liu L, Qi X, Chen Z, et al. Targeting the IRE1α/XBP1 and ATF6 arms of the unfolded protein response enhances VEGF blockade to prevent retinal and choroidal neovascularization. *Am J Pathol*. 2013; 182:1412-1424.
32. Keane PA, Patel PJ, Liakopoulos S, et al. Evaluation of age-related macular degeneration with optical coherence tomography. *Surv Ophthalmol*. 2012; 57:389-414.
33. Wang Q, Lin X, Xiang W, et al. Assessment of laser induction of Bruch's membrane disruption in monkey by spectral-domain optical coherence tomography. *Br J Ophthalmol*. 2015; 99:119-124.
34. Onami H, Nagai N, Machida S, et al. Reduction of laser-induced choroidal neovascularization by intravitreal vasohibin-1 in monkey eyes. *Retina*. 2012; 32:1204-1213.
35. Koinzer S, Saeger M, Hesse C, et al. Correlation with OCT and histology of photocoagulation lesions in patients and rabbits. *Acta Ophthalmol*. 2013; 91:e603-611.
36. Liu T, Hui L, Wang YS, et al. In-vivo investigation of laser-induced choroidal neovascularization in rat using spectral-domain optical coherence tomography (SD-OCT). *Graefes Arch Clin Exp Ophthalmol*. 2013; 251:1293-1301.
37. Jiao J, Mo B, Wei H, Jiang YR. Comparative study of laser-induced choroidal neovascularization in rats by paraffin sections, frozen sections and high-

resolution optical coherence tomography. *Graefes Arch Clin Exp Ophthalmol*. 2013; 251:301-307.

38. Berger A, Cavallero S, Dominguez E, et al. Spectral-domain optical coherence tomography of the rodent eye: highlighting layers of the outer retina using signal averaging and comparison with histology. *PLoS One*. 2014; 9:e96494.
39. Hoerster R, Muether PS, Vierkotten S, et al. In-vivo and ex-vivo characterization of laser-induced choroidal neovascularization variability in mice. *Graefes Arch Clin Exp Ophthalmol*. 2012; 250:1579-1586.

Figure Legends

Figure 1. Determination of ellipsoid axes in Micron OCT images. A) Representative images showing the horizontal plane of OCT imaging (*red line*) in the bright field fundus photographs and the radii *a* (width) & *b* (depth relative to the retina) on the corresponding zoomed in OCT scan. B) Representative images showing the vertical plane in the bright field image and radius *c* (length) on the corresponding orthogonal zoomed in OCT scan. C) A schematic diagram showing an ellipsoid with labeled axes corresponding to the OCT images, and the equation used in calculating ellipsoid volume. Scale bars = 100 μm. Abbreviations; ganglion cell layer (GCL), outer nuclear layer (ONL), retinal pigment epithelium (RPE).

Figure 2. L-CNV lesion volumes calculated from Micron OCT images obtained 14 days post-laser, analyzed by two independent graders, correlate with those calculated based on choroidal flatmount Z-stacks. Grader 1 (*left*) Spearman's $\rho = 0.79$, $P<0.01$. Grader 2 (*right*) $\rho = 0.78$, $P<0.05$. n = 10.

Figure 3. Choroidal flatmounts stained with agglutinin show a significant reduction in CNV lesion volume after anti-VEGF treatment. A) Representative images from confocal microscopy for CNV lesions from vehicle-treated (*left*) and anti-VEGF-treated eyes (*right*). Scale bars = 50 μm. B) Quantification of the CNV lesion volume from Z-stack images using ImageJ software demonstrated a significant reduction in CNV lesion volume after anti-VEGF intravitreal injection compared to vehicle treated controls, **$P<0.01$, Mann-Whitney test. Mean ± SEM, n = 6.

Figure 4. Quantification of L-CNV lesions by OCT shows a significant reduction in lesion volume after anti-VEGF treatment. A) Representative images of L-CNV lesions, shown between red brackets, from vehicle-treated (*left*) and anti-VEGF-treated eyes (*right*) obtained after 7 days (*top*) and 14 days (*bottom*). B) Quantification of the CNV lesion volume calculated as an ellipsoid, showing a significant reduction in CNV lesion volume after anti-VEGF intravitreal injection compared to vehicle treated controls, after both 7 and 14 days, with **P<0.01, Mann-Whitney test. Note different *y*-axis scales. Mean ± SEM, n = 6.

Figure 5. L-CNV lesion volumes following treatments calculated from Micron OCT images correlate with those calculated based on choroidal flatmount Z-stacks. (A) OCT calculations at 7 days, Spearman's ρ = 0.82. (B) OCT calculations at 14 days, ρ = 0.82. Vehicle-treated, blue, and anti-VEGF-treated eyes, red. P<0.01, n = 6 per treatment. Note different *y*-axis scales.

Figure 6. L-CNV lesion volumes calculated from InVivoVue OCT images obtained 10 days post-laser correlate with those calculated based on choroidal flatmount Z-stacks. A) Representative images showing the horizontal plane of OCT imaging (*green line*) in the en face image and the corresponding B-scan focus on the optic nerve head (ONH). Scale bar = 34 μm. B) Representative images showing the en face image and the corresponding B-scan at an L-CNV lesion (*arrow*). C) A significant correlation is

Sulaiman, R.S.

observed between 3D measurements of OCT images and confocal Z-stack images, Spearman's $\rho = 0.75$, $P<0.05$, $n = 10$.

Figure 1

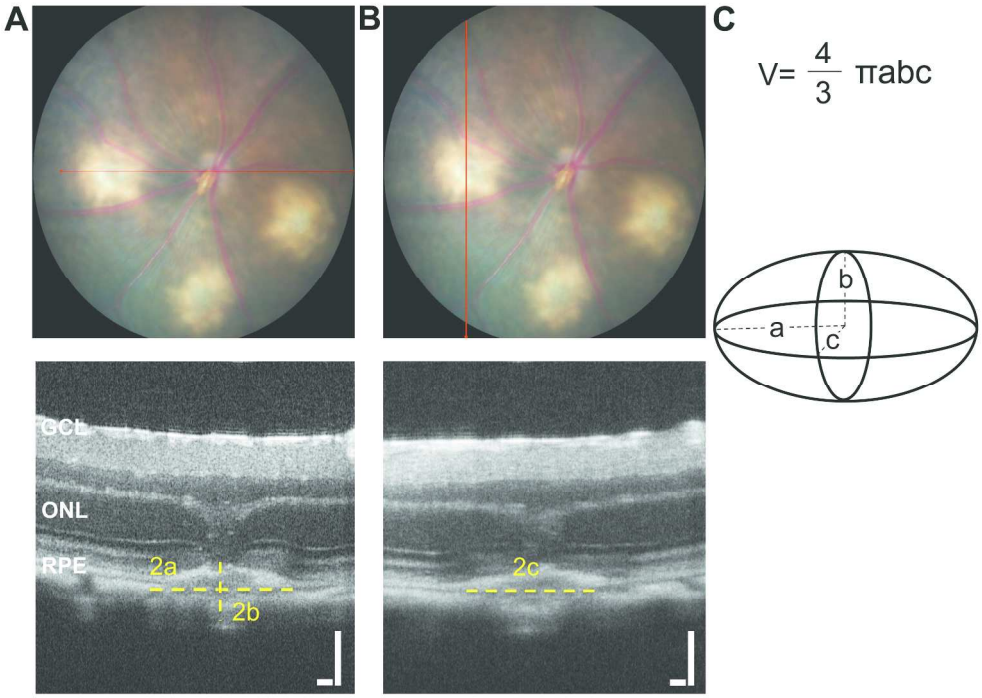

Figure 1. Determination of ellipsoid axes in Micron OCT images. A) Representative images showing the horizontal plane of OCT imaging (red line) in the bright field fundus photographs and the radii a (width) & b (depth relative to the retina) on the corresponding zoomed in OCT scan. B) Representative images showing the vertical plane in the bright field image and radius c (length) on the corresponding orthogonal zoomed in OCT scan. C) A schematic diagram showing an ellipsoid with labeled axes corresponding to the OCT images, and the equation used in calculating ellipsoid volume. Scale bars = 100 µm. Abbreviations; ganglion cell layer (GCL), outer nuclear layer (ONL), retinal pigment epithelium (RPE).
254x190mm (300 x 300 DPI)

Figure 2

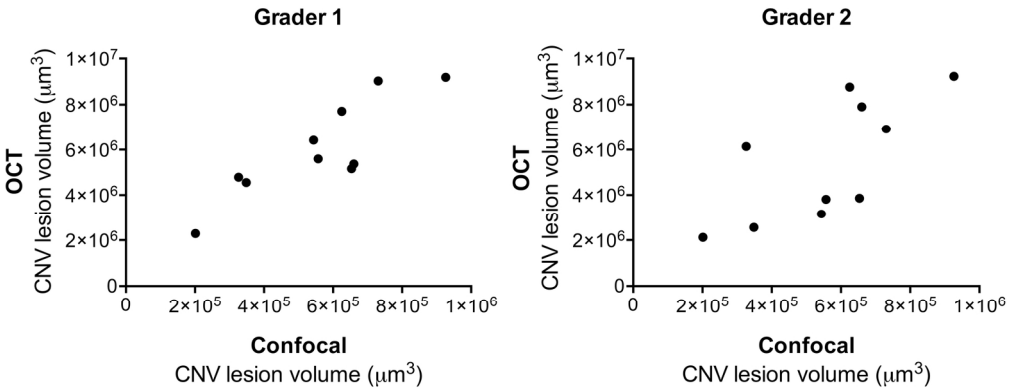

Figure 2. L-CNV lesion volumes calculated from Micron OCT images obtained 14 days post-laser, analyzed by two independent graders, correlate with those calculated based on choroidal flatmount Z-stacks. Grader 1 (left) Spearman's $\rho = 0.79$, $P<0.01$. Grader 2 (right) $\rho = 0.78$, $P<0.05$. $n = 10$.
82x35mm (600 x 600 DPI)

Figure 3

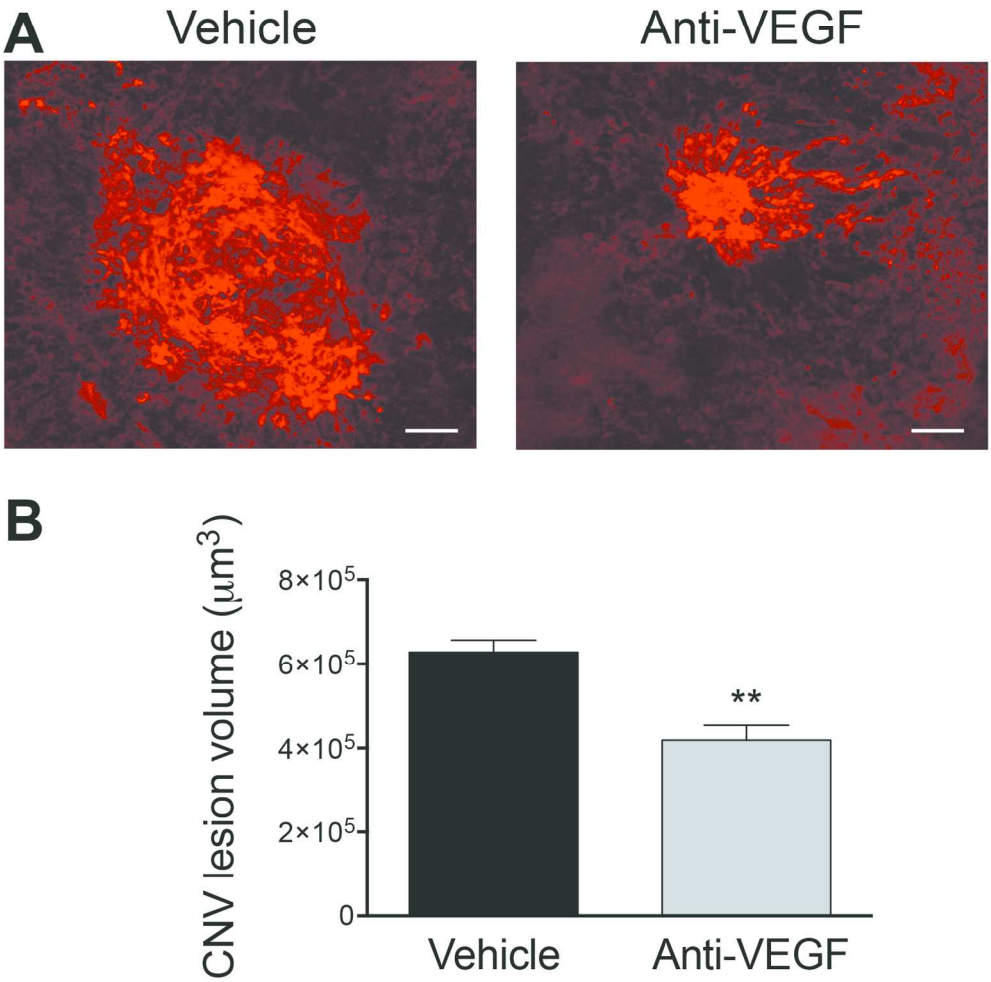

Figure 3. Choroidal flatmounts stained with agglutinin show a significant reduction in CNV lesion volume after anti-VEGF treatment. A) Representative images from confocal microscopy for CNV lesions from vehicle-treated (left) and anti-VEGF-treated eyes (right). Scale bars = 50 μm. B) Quantification of the CNV lesion volume from Z-stack images using ImageJ software demonstrated a significant reduction in CNV lesion volume after anti-VEGF intravitreal injection compared to vehicle treated controls, **P<0.01, Mann-Whitney test. Mean ± SEM, n = 6.
150x160mm (300 x 300 DPI)

Figure 4

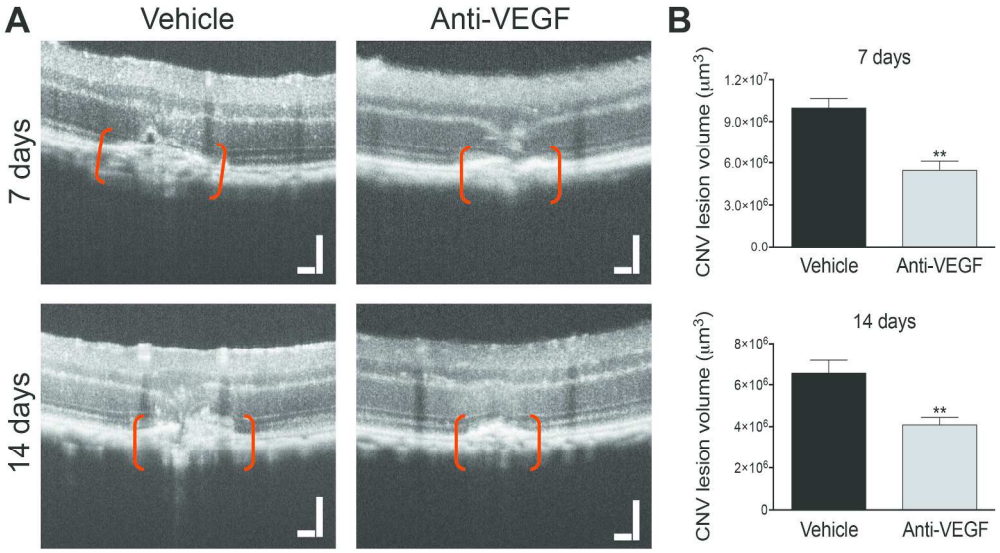

Figure 4. Quantification of L-CNV lesions by OCT shows a significant reduction in lesion volume after anti-VEGF treatment. A) Representative images of L-CNV lesions, shown between red brackets, from vehicle-treated (left) and anti-VEGF-treated eyes (right) obtained after 7 days (top) and 14 days (bottom). B) Quantification of the CNV lesion volume calculated as an ellipsoid, showing a significant reduction in CNV lesion volume after anti-VEGF intravitreal injection compared to vehicle treated controls, after both 7 and 14 days, with **P<0.01, Mann-Whitney test. Note different y-axis scales. Mean ± SEM, n = 6.
240x146mm (300 x 300 DPI)

Figure 5

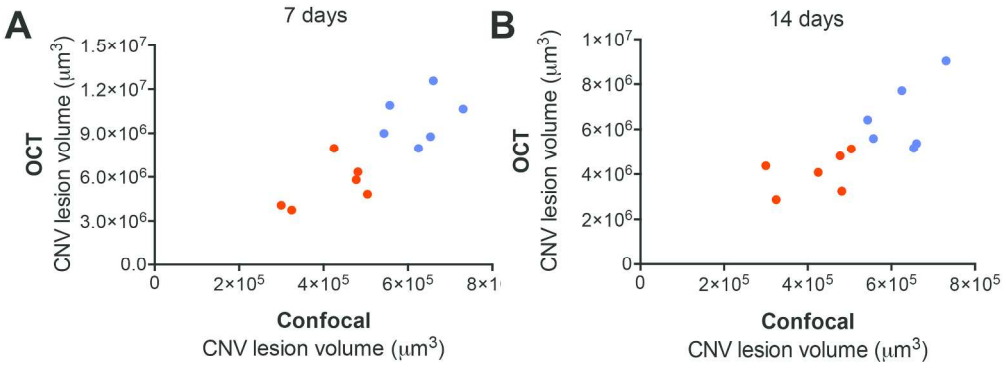

Figure 5. L-CNV lesion volumes following treatments calculated from Micron OCT images correlate with those calculated based on choroidal flatmount Z-stacks. (A) OCT calculations at 7 days, Spearman's ρ = 0.82. (B) OCT calculations at 14 days, ρ = 0.82. Vehicle-treated, blue, and anti-VEGF-treated eyes, red. P<0.01, n = 6 per treatment. Note different y-axis scales.
225x96mm (300 x 300 DPI)

Figure 6

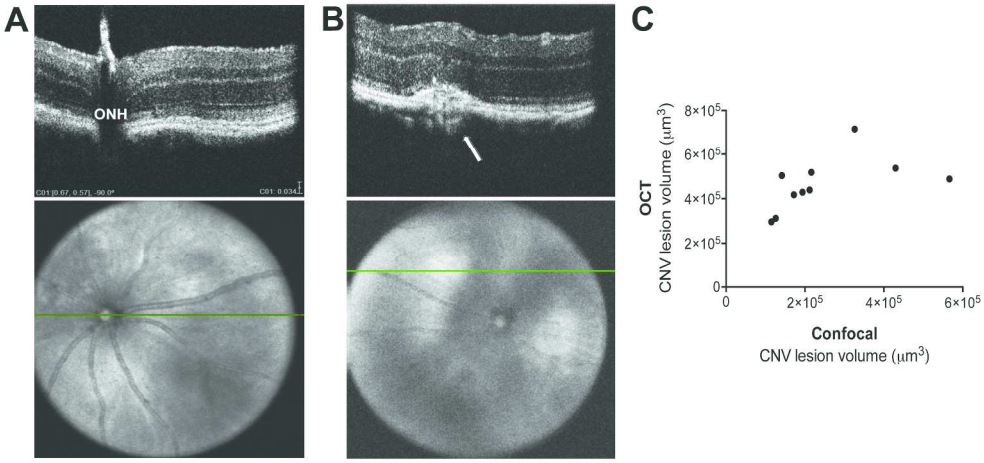

Figure 6. L-CNV lesion volumes calculated from InVivoVue OCT images obtained 10 days post-laser correlate with those calculated based on choroidal flatmount Z-stacks. A) Representative images showing the horizontal plane of OCT imaging (green line) in the en face image and the corresponding B-scan focus on the optic nerve head (ONH). Scale bar = 34 μm. B) Representative images showing the en face image and the corresponding B-scan at an L-CNV lesion (arrow). C) A significant correlation is observed between 3D measurements of OCT images and confocal Z-stack images, Spearman's $\rho = 0.75$, $P<0.05$, $n = 10$.
254x136mm (300 x 300 DPI)